Desalination and Water Treatment
www.deswater.com
doi: 10.5004/dwt.2021.27497

(2021) 149–164

Removal of Ni(II) from aqueous solutions by sulfide-modified nanoscale zero-valent iron supported by hydroxyapatite (HAP/S-nZVI)

Hui Xu*, Minzhang Chen, Yajuan Zhang, Pengdong Chen, Yong Chen*

College of Petrochemical Technology, Lanzhou University of Technology, Lanzhou, China, Tel. +86-931-2975872; emails: xuhui@lut.cn (H. Xu), chenylut@126.com (Y. Chen), 1377380676@qq.com (M. Chen), 1799797925@qq.com (Y. Zhang), 1214751712@qq.com (P. Chen)

Received 24 February 2021; Accepted 2 June 2021

ABSTRACT

Sulfide-modified nanoscale zero-valent iron (S-nZVI) has been widely used to remove various contaminants due to its excellent reactivity and selectivity. In this study, hydroxyapatite-supported sulfide-modified nZVI (HAP/S-nZVI) was synthesized and applied for Ni(II) elimination. The excellent performances of HAP/S-nZVI in Ni(II) removal showed that 98.25% of Ni(II) were removed using HAP/S-nZVI (1:0.5) after 15 min, much higher than HAP, nZVI and other adsorbents, and maximum adsorption capacity reached 302.27 mg g^{-1} at pH = 7 and 298 K. The morphology and structure of HAP/S-nZVI (1:0.5) composites were characterized by X-ray diffraction, X-ray photoelectron spectroscopy and transmission electron microscopy and other techniques, which verified the high disperse and activity of nZVI after sulfide-modified and supported by HAP. Furthermore, the stability study confirmed that the sulfide-modified nZVI can retain high Ni(II) removal efficiency than that of pristine nZVI after storage 60 d due to such powerfully protective layers of FeS_x synthesized during the sulfide modification. The pseudo-second-order kinetic model and Freundlich isotherm model more conform to describe the removal of Ni(II). The dynamic adsorption experiments further illustrated its potential ability for real applications.

Keywords: Sulfur-modified; Nano zero-valent iron; Hydroxyapatite; Removal; Ni(II)

1. Introduction

At present, the world is faced with the major problem of water pollution, due to the lack of appropriate sewage treatment technology, many developing countries are facing the challenge [1]. Especially the accumulation of heavy metals in the environment causes serious harm to human health, which deserves our attention [2]. Nickel (Ni) widely exists in water in the form of Ni(II), and direct contact can result in allergies, skin dermatitis and other diseases [3]. Hence, it is of great necessity to remove nickel from the water before consumption. There is a host of ways to remove Ni(II) from previous research, such as electrodeposition [4,5], chemical precipitation [6,7], ion flotation [8,9], adsorption [10,11] and microbial electrolysis cell methods [12]. Different methods have reduced the metal levels in the outfall, but the complete removal of metals is not guaranteed. It is exceedingly necessary to find a simple and economical approach to eliminate Ni(II) efficiently and widely.

Nano zero-valent iron (nZVI) has attracted extensive attention due to its low toxicity, high activity and low cost. nZVI has a stronger adsorption capacity than the traditional adsorbent and can absorb a variety of pollutants, including metals, dyes and organic matters [13,14]. However, nZVI can be limitedly used in the practical application for pollutant elimination due to its easy aggregation and

* Corresponding authors.

poor stability [15]. In order to promote the dispersion and anti-oxidation capability of nZVI particles, surface passivation and dispersion technology were applied for nZVI modification in recent years. Among the surface passivation technologies, sulfide-modified nanoscale zero-valent iron (S-nZVI) has stronger reducibility, better electron selectivity, the wide application range of pH and stability than nZVI, which greatly improves the problem of easy aggregation and passivation of nZVI and reduces the toxicity of nZVI [16]. Most studies have also shown that S-nZVI can remove heavy metals very effectively, such as Cr(VI), Cd(II), Sb(III) and U(VI) [17–20]. But the advantages of this material are not fully utilized at present, and S-nZVI is rarely applied for Ni(II) elimination.

The choice of a stable substrate for loading nZVI is also a particularly important solution to increasing its dispersion and stabilization. Hydroxyapatite (HAP) is a novel adsorption material in environmental remediation, due to its special structural features as well as good biocompatibility and biodegradability [21], it has been being used as an eco-friendly functional adsorbent for the removal of heavy metal ions [22], antibiotics [23] and organic compounds [24,25] in aqueous effluents recently. However, HAP exhibits poor performances such as long adsorption time, low adsorption capacity and bad reusability. A feasible approach is to use the HAP as a stable substrate for loading nZVI and make HAP with abundant active sites to improve its adsorption efficiency. It has been reported that HAP can be a carrier to improve the dispersion of nanoparticles [26]. The composite can be applied to the environmental remediation treatment combined with excellent adsorption property and strong reducibility of nZVI.

In this study, HAP/S-nZVI materials were synthesized by liquid phase one-step synthesis and applied as neotype adsorbent for Ni(II) removal from wastewater. During the preparation process, Fe(II) is first reduced to Fe^0, due to $Na_2S_2O_4$ is not stable, it breaks down and releases H_2S, reacts with the generated Fe^0 to produce insoluble FeS on its surface. The reaction proceeded according to the following equations [27,28]:

$$Fe^{2+} + 2BH_4^- + 6H_2O \rightarrow Fe^0 + 2B(OH)_3 + 7H_2 \quad (1)$$

$$2S_2O_4^{2-} + 4H^+ \rightarrow 3SO_2 + S^0 + 3H_2O \quad (2)$$

$$2S_2O_4^{2-} + H_2O \rightarrow S_2O_3^{2-} + 2HSO_3^{2-} \quad (3)$$

$$S_2O_4^{2-} + S_2O_3^{2-} + 2H_2O + H^+ \rightarrow 3HSO_3^{2-} + H_2S \quad (4)$$

$$Fe^{2+} + H_2S \rightarrow FeS + 2H^+ \quad (5)$$

$$Fe^0 + S^0 \rightarrow FeS \quad (6)$$

The main object of the paper was (1) To evaluate the removal performance of Ni(II) on HAP/S-nZVI composite by batch experiments (the different single factor, isotherms and thermodynamic studies, stability, etc); (2) To characterize the surface properties of HAP/S-nZVI before and after elimination Ni(II) and propose feasible removal mechanisms.

2. Materials and methods

2.1. Chemical reagents

Hydroxyapatite (HAP, 97% purity), sodium borohydride ($NaBH_4$, 98% purity), ferrous sulfate ($FeSO_4·7H_2O$), nickel nitrate ($Ni(NO_3)_2$), dithionite ($Na_2S_2O_4$), sodium hydroxide (NaOH) and hydrochloric acid (HCl), iodine, potassium iodide (KI), ammonium citrate, dimethylglyoxime, ethylenediaminetetraacetic acid (EDTA). All the chemicals were analytical grade and were used without further purification. Deionized water was used for all reagents and materials preparation.

2.2. Preparation of nZVI and HAP/S-nZVI

HAP-supported S-nZVI composites with HAP/S-nZVI mass ratio of 1:1 were prepared using the liquid-phase reduction method [16]. Briefly, 100 mL mixed suspension of HAP (1 g) and $FeSO_4·7H_2O$ (0.018 M) was dispersed by ultrasound, to avoid oxidation N_2 was continued to pass into the above flask to drive the air away under mechanical stirring. After 30 min, the 100 mL mixed solutions of $NaBH_4$ (0.054 M) and $Na_2S_2O_4$ (0.0045 M) were introduced drop by drop, which prescribed the synthesized HAP/S-nZVI with a S/Fe molar ratio of 0.5, it was stirred for 1 h. Different doses of $Na_2S_2O_4$ were slowly introduced into the solution to achieve S/Fe ratios of 0.1, 0.3 and 0.5. Finally, after filtrating, the obtained products were quickly rinsed several times with deionized water and pure ethanol in a vacuum oven at 60°C for 6 h. The whole process is under the protection of N_2. Similarly, the nZVI and HAP/nZVI used were prepared by the same method.

2.3. Batch experiments

Batch experiments were carried out at room temperature (25°C) in 250 mL flasks, each flask contained 100 mg HAP/S-nZVI with S/Fe molar ratio of 0.5 and 100 mL of 50 mg L^{-1} Ni(II) solution, and the suspension was agitated by the constant temperature oscillating shaker (230 rpm) at pH = 7.0 and 298 K. During stirring, 1 mL samples were taken at different times (1, 3, 5, 10, 20, 40, 60 min) and filtered through filter paper before being analyzed. The absorbance of nickel ions in the absorbable solution at λ = 530 nm is determined using an ultraviolet spectrophotometer. All experiments were repeated three times and averaged.

The removal ability of Ni(II) was compared with that of nZVI and HAP/nZVI by using HAP/S-nZVI with different S/Fe molar ratios (0.1, 0.3 and 0.5). In addition, the effects of different initial concentrations (25–100 mg L^{-1}), different pH values (3–9), and different dosages (50–150 mg L^{-1}) on the removal rate of Ni(II) were studied. The effects of different temperatures (303, 313, and 323 K) and different concentrations (25–100 mg L^{-1}) on the adsorption thermodynamics and various kinetic parameters of Ni(II) removal were studied. And calculate the removal rate (R) and adsorption capacity (q) [Eqs. (7) and (8)]:

$$R = \frac{c_0 - c_t}{c_0} \times 100\% \quad (7)$$

$$q = \frac{c_0 - c_t}{m} \times V \tag{8}$$

where $R(\%)$ is the removal efficiency of the pollutants; q is the adsorption capacity of the dye at t mins; c_0 and c_t are the initial concentration of the pollutant solution and the concentration at t min (mg L^{-1}), respectively; V is the volume of the adsorbate solution (L); m is the mass of the adsorbent (g).

Ni(II) detection method: 1 mL of a water sample is taken and placed in a 50 mL calorimetric tube, add 50% ammonium citrate 2.0 mL and 0.05 mol L^{-1} iodine solution 1.0 mL successively, then add water to 20 mL and shake well. 2.0 mL of 0.5% diacetyloxime solution and 2.0 mL of 5% Na_2-EDTA (disodium ethylenediaminetetraacetate) solution were introduced in sequence, and water was added to the mark and shaken. Let it stand for 5 min and measure the absorbance value at λ = 530 nm.

2.4. Characterization analyses

The hydrophilicity and hydrophobicity of nZVI and S-nZVI were analyzed with a contact angle measuring instrument (DSA100, Germany). Surface morphology and elementary composition of the nZVI and HAP/S-nZVI were observed by scanning electron microscope (SEM, MIRA3 TESCAN) and transmission electron microscopy (TEM, JEM-1200EX, USA), in conjunction with energy-dispersive X-ray spectroscopy (EDX). The composite structure was analyzed by X-ray powder diffraction (D/MAX-2400X, Rigaku D/max, Japan, the scanning speed was 4°/min, the voltage was 44 KV, and the current was 150 mA). Fourier transform-infrared spectroscopy (FTIR, NEXQS670, USA) was used to identify the functional groups of nZVI, HAP and HAP/S-nZVI composite (before and after reaction) over a wavenumber range from 500 to 4,000 cm^{-1}. Surface electronic states were observed by using X-ray photoelectron spectroscopy (XPS). A Zetasizer Nano ZS (Malvern Instruments, UK) was used to determine the zeta potentials of HAP/S-nZVI particles.

3. Results and discussion

3.1. Method optimization

3.1.1. Ni(II) removal with different adsorption materials

Ni(II) removal efficiencies of HAP/S-nZVI were compared with other adsorption materials in Fig. 1a. The removal efficiency of a single HAP is 79.83% after 60 min, which indicates that HAP has good adsorption ability just on itself [21,32]. Moreover, regardless of the mass ratio of S/Fe, the removal efficiency of HAP/S-nZVI is higher than HAP, nZVI and HAP/nZVI, which can reach 97.80%, 97.75% and 98.24% after 15 min, respectively. And the adsorption equilibrium time is shorter than that of a single adsorbent and HAP/nZVI. Further comparing the removal efficiency of three HAP/S-nZVI and HAP/nZVI, we can draw conclusions that S-nZVI in composites play an important role in Ni(II) removal and more sulfur modified nZVI in composites can provide much higher removal efficiency. In particular, HAP/S-nZVI can provide much higher removal efficiency at the beginning because of the higher removal instantaneous speed as shown in Table S1. These results indicate that the sulfur-modified nZVI can promote the transfer of electrons and remove Ni(II) more effectively. According to the literature [17,18], FeS synthesized during the sulfide modification is a key factor for the enhancement reactivity of nZVI. First, The presence of the FeS layer promotes electron conduction from Fe^0 to contaminants [33]. The conclusion was also verified by electrochemical analysis of nZVI and S-nZVI. As shown in the Tafel curve (Fig. 1b), S-nZVI has a higher corrosion current (3.617×10^{-3} A) compared to the bare nZVI (1.385×10^{-3} A), which shows that the sulfidation may obtain better overall rates of electron transfer and more beneficial to the removal of Ni(II) [34]. In addition, sulfidation modification might effectively alleviate the loss of reducing capacity during interaction with water, thus improving the efficiency of electron transfer from nZVI to pollutants, Fig. S1 can be used to prove the conclusion [35]. In the subsequent studies, the S/Fe mass ratio of 0.5 is chosen as the optimum mass ratio.

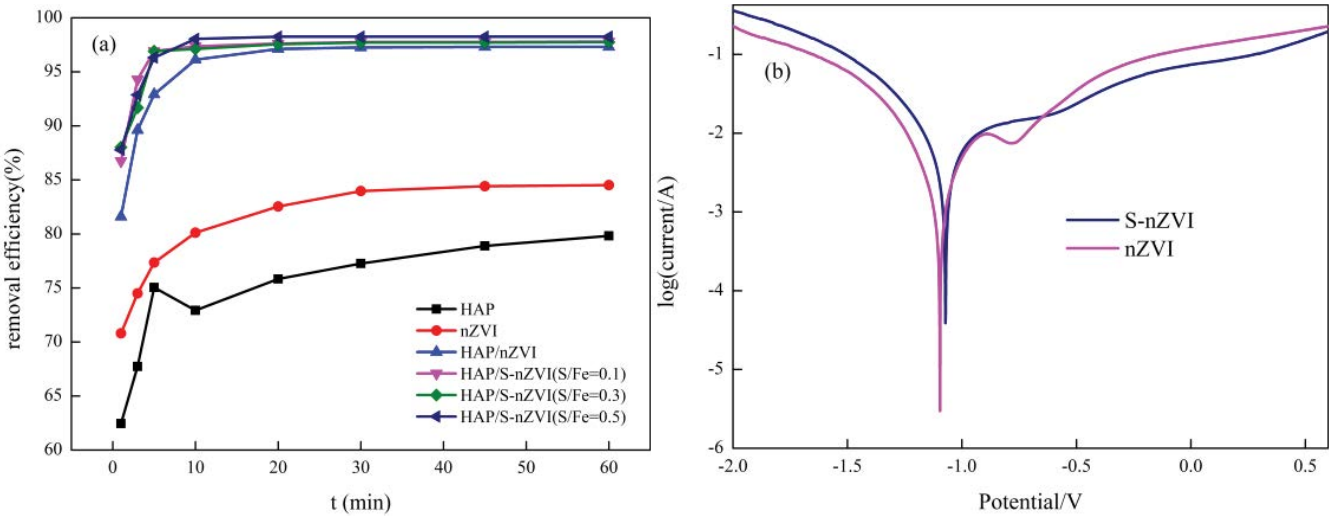

Fig. 1. (a) Effects of adsorption materials and (b) Tafel profiles for S-nZVI and bare nZVI.

3.1.2. Effect of HAP/S-nZVI dose on Ni(II) removal performance

The impact of the HAP/S-nZVI dosage (0.05–0.15 g 100 mL) on the removal reaction was determined (Fig. 2a). When more HAP/S-nZVI is utilized from 0.5, 1.0 to 1.5 g L^{-1}, the corresponding removal efficiency is 94.84%, 98.25% and 97.85% and the adsorption capacity is 97.60, 49.12 and 32.62 mg g^{-1} after reached equilibrium. The possible reason is that higher composite material dosages can provide more active sites, thereby increasing the removal efficiency of Ni(II).

3.1.3. Effect of HAP/S-nZVI initial concentration on Ni(II) removal performance

The effect of the initial concentration of Ni(II) on heavy metal Ni(II) removal is shown in Fig. 2b. It can be observed that the removal efficiency and the reaction speed of Ni(II) decreased with an increase in the initial concentration of Ni(II). When the initial concentration changes from 25 to 100 mg L^{-1}, the removal efficiency decreases from 98.2% to 97.65%, the removal efficiency is not significantly reduced, indicating a larger removal capacity for the composite. Since the available adsorption sites on HAP/S-nZVI were fixed, more adsorption sites were required for the complete removal with the increase of concentration, which led to the decrease of removal efficiency at higher concentrations. Similar phenomena have been observed in other studies [36].

3.1.4. Effect of pH on Ni(II) removal performance

The pH value of common groundwater usually ranges from 4.0 to 9.0 [37]. Ni(II) will exist in the form of precipitation when pH > 9. In order to verify the material in the acidic environment of the adsorption performance, we select pH from 3.0–9.0 to assess the pH effect on the removal of Ni(II) by HAP/S-nZVI. The result is shown in Fig. 2c. The removal efficiency remains above 96% as solution pH increases from 3 to 9, indicating that HAP/S-nZVI

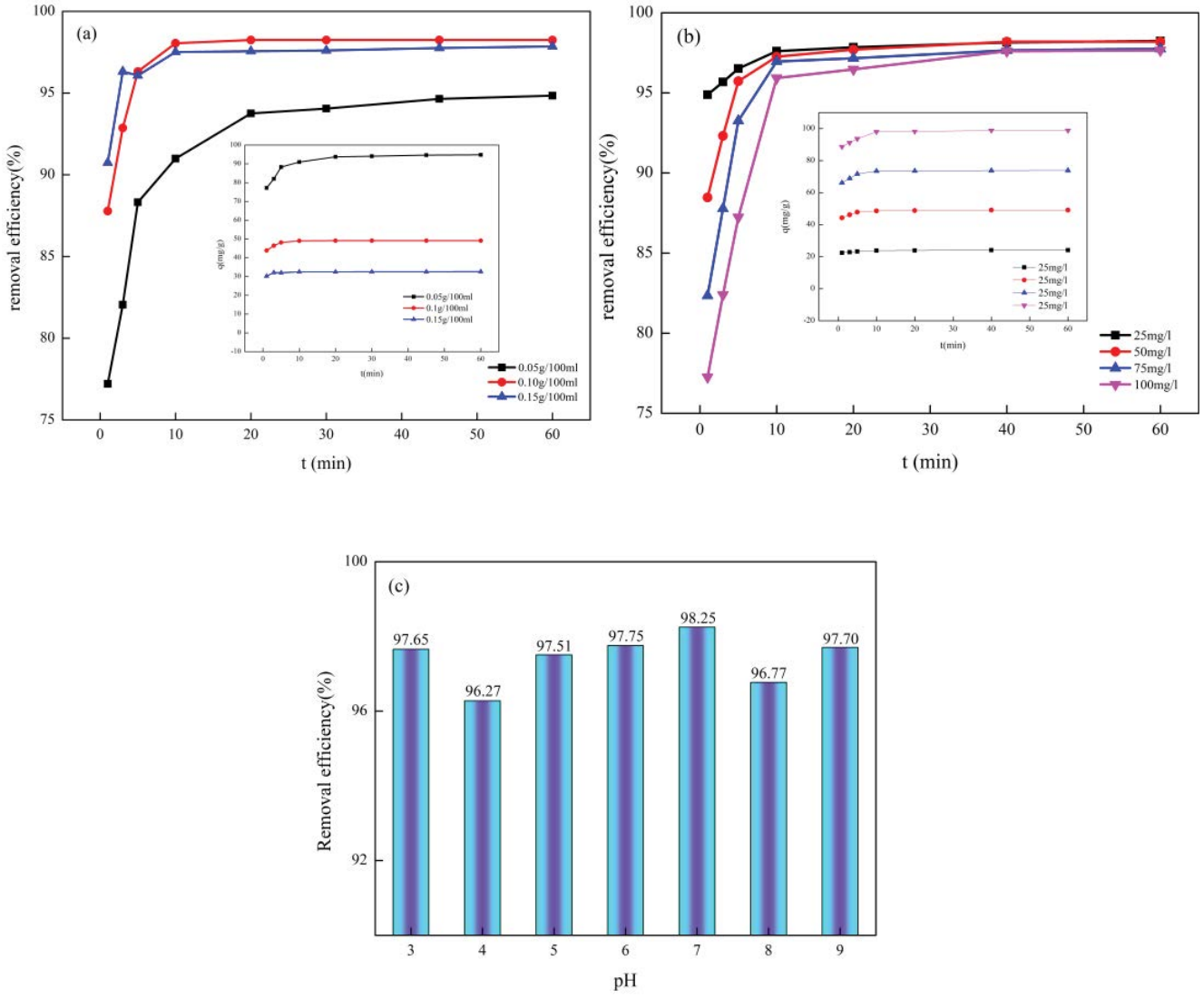

Fig. 2. (a) Composite material dose, (b) Ni(II) initial concentration and (c) pH on the Ni(II) removal capacity of HAP/S-nZVI.

has excellent adsorption property within a wider pH range. The possible reason is that under acidic conditions, H^+ would significantly accelerate the corrosion of nZVI and promote the dissolution of surface oxides into Fe^{2+}, and the iron element will be exposed to produce more active sites, which is a key step in the removal of Ni(II). According to zeta potential of HAP/S-nZVI shown negative value at pH = 3–9 in Fig. S2, which is attributed to the presence of FeS on the surface of the HAP/S-nZVI particles, it can be obtained from previous studies [38]. The conclusion can be illustrated that there are electrostatic attractions between adsorbents and adsorbates. Under alkaline conditions, Ni(II) combines with OH^- in the solution and exists as a precipitate, also beneficial to the removal of Ni(II).

3.2. Stability of nZVI, HAP/nZVI and HAP/S-nZVI for Ni(II) removal

Because the surface of nZVI is easily oxidized by air to further reduce its reactivity and increase toxicity, stability of the HAP/S-nZVI composite is an important property for evaluation of its practical usage [39]. Fig. 3 displays the activity of nZVI, HAP/nZVI and HAP/S-nZVI placed in air with different storage time. Obviously, it can be noted that the reactive activity of HAP/S-nZVI is always the largest in the three samples from beginning to 60 d. After exposed in the air 60 d, the removal efficiency of HAP/S-nZVI is still exceeded 91.77%. It indicates that the presence of FeS_x synthesized during the sulfide modification not only inhibited aggregation of nZVI but also protected nZVI from the oxidation by air [17], thus, a high reactivity of HAP/S-nZVI can be obtained. In addition, the activity of HAP/nZVI is higher than nZVI. It is further illustrated that supporter HAP also played an important role in maintaining the reactivity of nZVI. Table S2 summarized the adsorption performance of different adsorbents reported in other literature. It is worth noting that HAP/S-nZVI has higher removal efficiency, shorter adsorption equilibrium time and wide range of pH. Therefore, HAP/S-nZVI composites will be on track to apply in the contaminated water treatment.

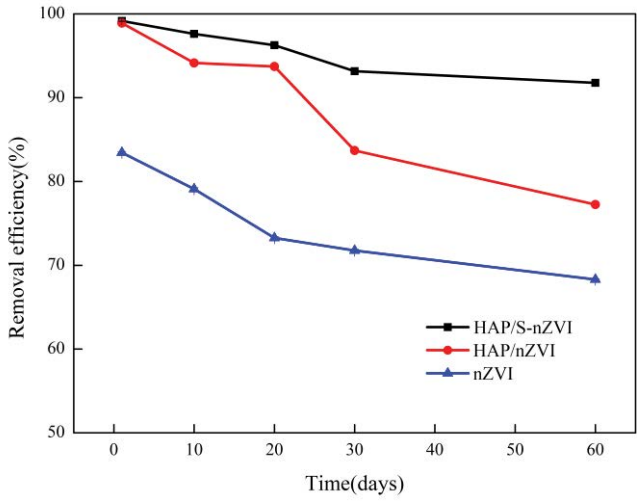

Fig. 3. Stability of nZVI, HAP/nZVI and HAP/S-nZVI for Ni(II) removal.

3.3. Dynamic adsorption of Ni(II)

In order to improve the role of composite materials in practical applications, we connected a dynamic adsorption device for the removal of Ni(II) (Fig. S3). In the case that other conditions remain unchanged, Ni(II) can be removed by changing the rotating speed of the peristaltic pump (at 25, 50, 75 and 100 rpm). Fig. 4 shows that a high removal efficiency (89.9%) can be obtained after 120 min of adsorption. Indicating the feasibility of the adsorbent in practical application. Different rotational speeds also have a certain effect on the removal of Ni(II). Too small rotation speed will lead to longer cycle time, which will lead to longer contact time between Ni solution and adsorbent. However, if the speed is too fast, the contact time between the adsorbent and the Ni solution will be shorter, but the time for a cycle will be shorter. Therefore, a suitable speed of 50 rpm is obtained.

3.4. Adsorption kinetics

The adsorption kinetics of Ni(II) removal by HAP/S-nZVI were studied over a range of initial concentrations (25–100 mg L^{-1}) at pH 7. As shown in Fig. 2c, the removal process was the fastest within the first 10 min and reached equilibrium around 15 min. To study the Ni(II) removal mechanism by HAP/S-nZVI. Both of the pseudo-first-order [Eq. (9)], pseudo-second-order [Eq. (10)] and intraparticle diffusion [Eq. (11)] models are widely used to analyze the kinetic data (Fig. S4), with the results summarized in Table 1.

$$\ln\left(q_e - q_t\right) = \ln q_e - k_1 t \tag{9}$$

$$\frac{t}{q_t} = \frac{1}{k_2 q_e^2} + \frac{t}{q_e} \tag{10}$$

$$q_i = k_{id} t^{1/2} + c_i \tag{11}$$

where q_t (mg g^{-1}) and q_e (mg g^{-1}) are the adsorption capacity at time t (min) and equilibrium, respectively. k_1 (min^{-1}) and

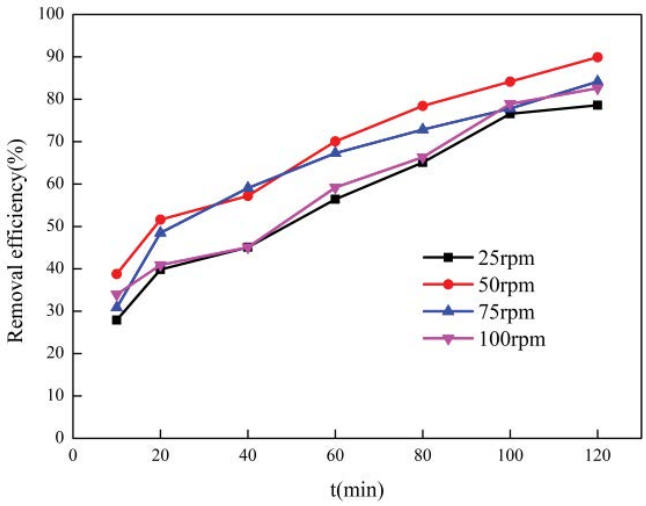

Fig. 4. The removal rate of Ni(II) at different rotating speeds.

Table 1
Kinetic parameters obtained from pseudo-first-order kinetic model and pseudo-second-order kinetic model for Ni(II) removal by HAP/S-nZVI at 298 K

		Pseudo-first-order			Pseudo-second-order			Intraparticle diffusion		
c_0 (mg L^{-1})	q_e (mg g^{-1})	q_e	k_1	R^2	q_e	k_2	R^2	q_e	k_3	R^2
25	24	23.90	0.0978	0.9585	24	0.3479	1	22.8	0.1866	0.6332
50	48.90	48.49	0.0555	0.6859	48.97	0.1668	0.9999	47.17	0.2533	0.8587
75	73.88	70.54	0.0793	0.6905	74.07	0.0715	0.9999	68.87	0.7657	0.6530
100	98.83	94.58	0.1324	0.9695	99	0.0857	1	94.09	0.7364	0.7243

k_2 (g mg^{-1} min^{-1}) is the kinetic rate constant for the pseudo-first-order and pseudo-second-order models. k_{id} is the intraparticle diffusion rate constant (g mg^{-1} min$^{-0.5}$); c_i is the thickness of the boundary layer.

As shown in Fig. S4a, adsorption process consists of three stages: (1) rapid adsorption of adsorbent surface; (2) slow adsorption; (3) adsorption equilibrium. The first 5 min were rapid adsorption phase and Ni(II) was adsorbed rapidly on the active sites of adsorbent. In 5–10 min for the slow adsorption process, accompanied by Ni(II) adsorption, echoed off the degradation. At the stage of adsorption equilibrium after 10 min, the active site on the surface of the adsorbent is completely occupied to achieve adsorption equilibrium. The experimental data basically conforms to the pseudo-second-order kinetic model. The kinetic parameters were determined using linear regression analysis and the results are presented in Table 1. The pseudo-second-order model provided a better fit (R^2 > 0.9999), and the calculated q_e is closest to the theoretical value. It can be inferred from this that the removal of Ni(II) by HAP/S-nZVI follows a pseudo-second-order kinetic model, the study of adsorption of Cd(II) or Cr(VI) on S-nZVI has also reached the same conclusion [18,28]. The results show that chemisorption mechanism was the rate-controlling step.

3.5. Reduction kinetics

Usually, two equations expressed below are used to describe reduction kinetics, which are also named as the pseudo-first-order and pseudo-second-order kinetic models, respectively, whose model is expressed as Eqs. (12) and (13). Additionally, the apparent activation energy (E_a) can be calculated by plotting the logarithm of K vs. $1/T$ according to the Arrhenius equation, which is described in Eq. (14) [40].

$$\ln\frac{c_t}{c_0} = -k_{obs1}t \tag{12}$$

$$\ln\left(\frac{1}{c_t}-\frac{1}{c_0}\right) = k_{obs2}t \tag{13}$$

$$\ln K_{obs} = -\frac{E_a}{RT} + \ln A \tag{14}$$

where c_t is the concentration of Ni(II) in t min and c_0 is the initial concentration; K_{obs1} and K_{obs2} (min^{-1}) is the kinetic rate constant for the pseudo-first-order kinetic and pseudo-second-order kinetic models, respectively. Where the apparent activation energy and the pre-exponential factor are expressed as E_a (kJ mol^{-1}). Specific fitting data are shown in Table 2.

In terms of the values of R^2 in Table 2, The results show that the reduction kinetics of Ni(II) can be better described by the pseudo-second-order model. With the decrease of the initial concentration, the values of K_{obs2} decreased from 0.0151 to 0.0122, indicating that the higher the initial concentration, the lower the degradation rate and the fewer active sites on the surface.

Moreover, the kinetic property of reaction can be always reflected by the value of E_a. The activation energy is 8.422 kJ mol^{-1} calculated by Eq. (17), indicating that the degradation of Ni(II) is controlled by diffusion. Since when E_a > 29 kJ mol^{-1}, the process is a surface-controlled reaction, while when 8 < E_a < 21 kJ mol^{-1}, the process is a diffusion-controlled reaction [41].

3.6. Adsorption isotherms

The adsorption isotherm of HAP/S-nZVI to Ni(II) was studied at different temperatures to understand the thermodynamic behavior and the possible adsorption mechanism during the removal process. Respectively using Langmuir [Eq. (15)], Freundlich [Eq. (16)], Liu [Eq. (17)] isothermal model research of Ni(II) removal process and the equations were displayed as follows:

$$q_e = \frac{q_m \cdot K_L \cdot c_e}{1 + K_L \cdot c_e} \tag{15}$$

$$q_e = K_F \cdot c_e^{1/n_F} \tag{16}$$

$$q_e = \frac{q_m \cdot \left(K_g \cdot c_e\right)^{n_L}}{1 + \left(K_g \cdot c_e\right)^{n_L}} \tag{17}$$

where q_e and c_e are the adsorption equilibrium adsorption capacity (mg g^{-1}) and Ni(II) concentration (mg L^{-1}) respectively; q_m is the theoretical maximum adsorption capacity (mg g^{-1}); K_L is the Langmuir constant (L mg^{-1}); K_F is the Freundlich constant (mg L^{-1}); K_g (L mg^{-1}) is the constant Liu equation. $1/n$ and n_L are the exponents of two equations.

According to Fig. S5 and Table 3, we could get the result of fitting model fitted by Freundlich model than the other

Table 2
Degradation kinetics parameters of degradation of Ni(II) by HAP/S-nZVI

		Pseudo-first-order model		Pseudo-second-order model	
T (K)	c_0 (mg g^{-1})	K_{obs1} (min^{-1})	R^2	K_{obs2} (min^{-1})	R^2
	50	0.0313	0.7110	0.0151	0.8866
298	75	0.0281	0.7641	0.0132	0.8991
	100	0.0269	0.6899	0.0122	0.8416
308	50	0.0336	0.9258	0.0152	0.8084
318	50	0.0252	0.5686	0.0174	0.9198

Table 3
Isotherm parameters of Ni(II) adsorption on HAP/S-nZVI

T (K)	298	308	318
Langmuir			
q_m (mg g^{-1})	302.27	287.23	274.71
K_L (L mg^{-1})	0.1057	0.1319	0.1603
R^2_{adj}	0.9834	0.9737	0.9533
SD (mg g^{-1})	30.66	31.74	35.5
Freundlich			
K_F (mg g^{-1}(mg L^{-1})$^{-1/n}$)	44.40	48.32	53.02
$1/n$	0.5130	0.4937	0.4664
R^2_{adj}	0.9962	0.9827	0.9602
SD (mg g^{-1})	3.02	6.53	10.09
Liu			
q_m (mg g^{-1})	335.36	315.22	289.33
K_g (L mg^{-1})	0.308	0.350	0.667
n_L	0.5352	0.5614	0.5561
R^2_{adj}	0.9950	0.9773	0.9474
SD (mg g^{-1})	19.47	46.15	42.02

two models and have higher values of R^2 and the lowest standard deviation of residues (SD) values, indicating that the adsorption process was multilayer and heterogeneous. Furthermore, the maximum adsorption capacities of HAP/S-nZVI were calculated to be 302.27, 287.23 and 274.71 mg g^{-1} at 298, 318 and 328 K, respectively.

3.7. Thermodynamic study

The thermodynamic parameters are significant factors determining feasibility of adsorption process. Including Gibbs free energy ($\Delta G°$), enthalpy ($\Delta H°$) and entropy ($\Delta S°$). The formula is as follows:

$$K_d = \frac{q_e}{c_e} \tag{18}$$

$$\Delta G° = -RT \ln K_d \tag{19}$$

$$\ln K_d = -\frac{\Delta H°}{RT} + \frac{\Delta S°}{R} \tag{20}$$

where R (8.314 J K^{-1} mol^{-1}) and T (K) indicate ideal gas constants and Kelvin temperatures respectively; K_d could be calculated from the slope of the plot of q_e vs. c_e, this in turn suggests that Eq. (18) would be a special case of the well-known Freundlich isotherm equation [42].

The calculated results are shown in Table 4. At different temperatures, the values of $\Delta G°$ are negative, which proves that adsorption processes are spontaneous. The value of $\Delta H°$ is positive, indicating that the adsorption process is an endothermic reaction. The increase of entropy ($\Delta S° > 0$) indicates that the degree of solid–liquid interface chaos increases.

3.8. Characterization of nZVI and HAP/S-nZVI particles

The surface morphology of the particles was observed by using a SEM. Fig. 5a shows that pure HAP has a granular structure with an average particle size of about 100nm, all of which are nanoscale [43]. The surface morphologies of nZVI are shown in Fig. 5b. Because of the high surface energy and electrostatic interaction, the nanometer zero-valent iron has a chain structure and aggregation state [37,40]. In the same magnifying scale, compared with nZVI, S-nZVI particle obviously has larger size and more dispersed than nZVI, and the typical chain-like structure of nZVI was not observed in S-nZVI (Fig. 5c). It is probably that FeS_x covers the surface of nZVI [18]. Fig. 5d shows that the introduction of HAP can increases the dispersion of S-nZVI particles, which is helpful to alleviate the aggregation of nZVI in practical applications.

TEM images of freshly prepared nZVI and HAP/S-nZVI are shown in Fig. 6. As shown in Fig. 6a, nano-sized spherical particles aggregating into a chain-like structure appeared in bare nZVI because of the higher surface energy and electrostatic interactions [44]. Compared with nZVI, the nZVI particles displayed a significant dispersion and evenly distributed after HAP loaded and sulfide modification (Fig. 6b), greatly reducing the agglomeration of nZVI and increasing the adsorption site. As seen in the EDX spectrum of nZVI and HAP/S-nZVI (illustration of Fig. 6), there are two major elements (Fe, O) distribution of nZVI, proving the formation of iron oxides [18]. S peak appeared in the EDX spectrum of HAP/S-nZVI confirmed the presence of S after sulfide modification, conforming the possible formation of FeS. Ca and P are elements in the HAP structure.

The structures of nZVI, HAP/nZVI and HAP/S-nZVI were evaluated through X-ray diffraction (XRD) analysis (Fig. 7). For nZVI, peaks at 2θ of 44.6° and 65.1° were

Table 4
Thermodynamic parameters of Ni(II) adsorption on HAP/S-nZVI

Temperature (K)	R^2	$\Delta H°$ (kJ mol^{-1})	$\Delta S°$ (J mol K^{-1})	$\Delta G°$ (kJ mol^{-1})
298	0.9962	5.30	41.17	–6.97
308	0.9827			–7.14
318	0.9602			–7.31

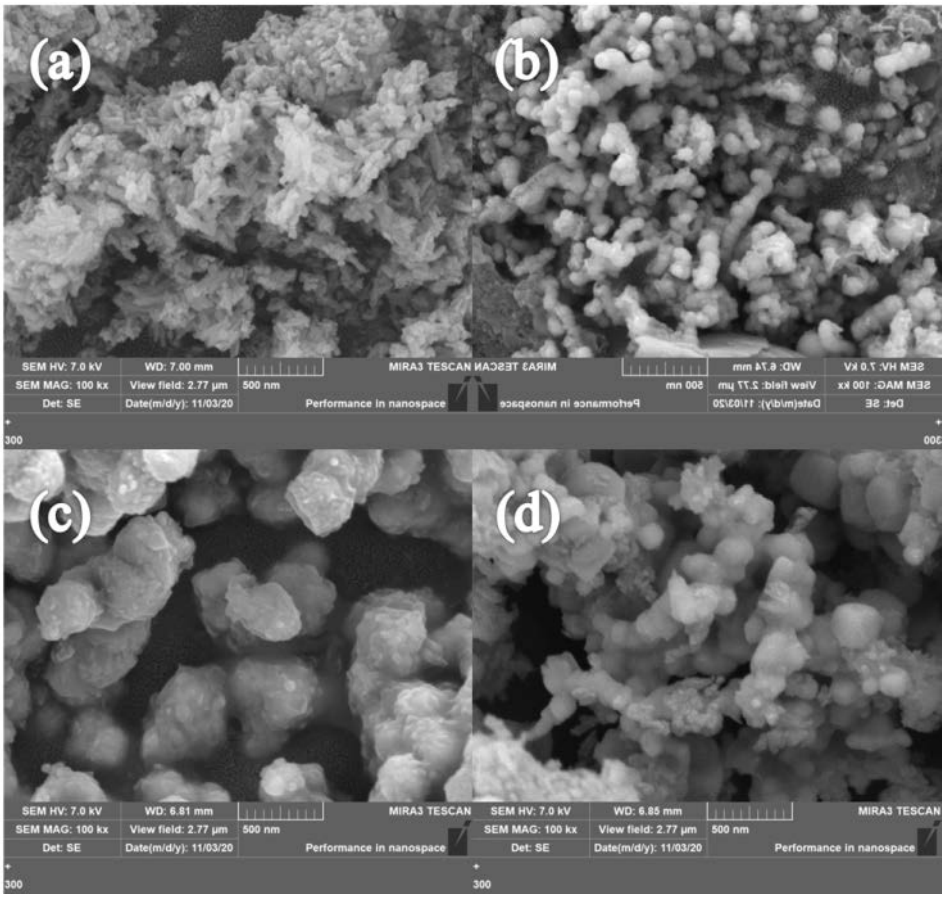

Fig. 5. Scanning electron microscope (SEM) images of (a) HAP, (b) nZVI, (c) S-nZVI and (d) HAP/S-nZVI particle.

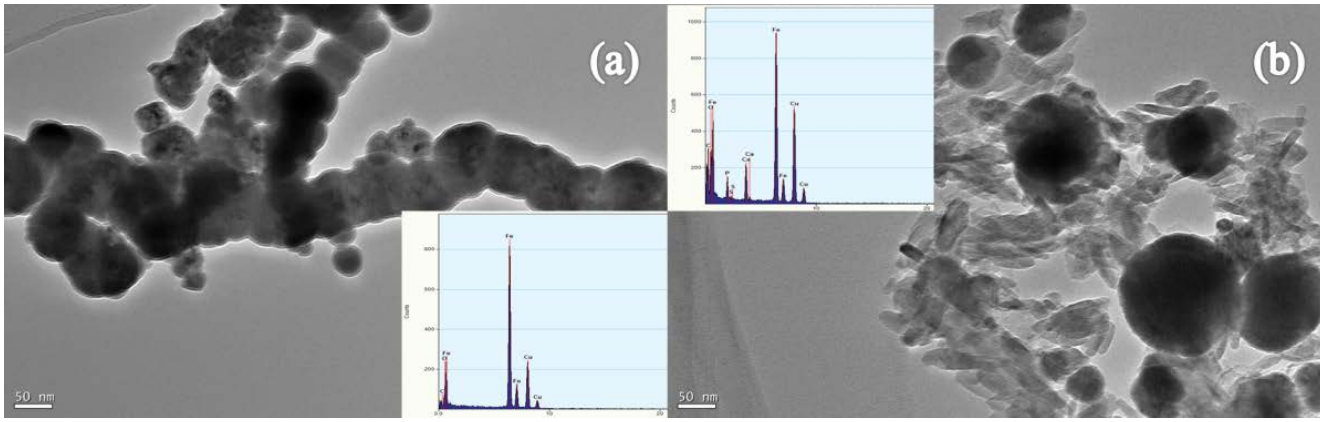

Fig. 6. (a) TEM images and EDX spectra of nZVI and (b) TEM images and EDX spectra of HAP/S-nZVI.

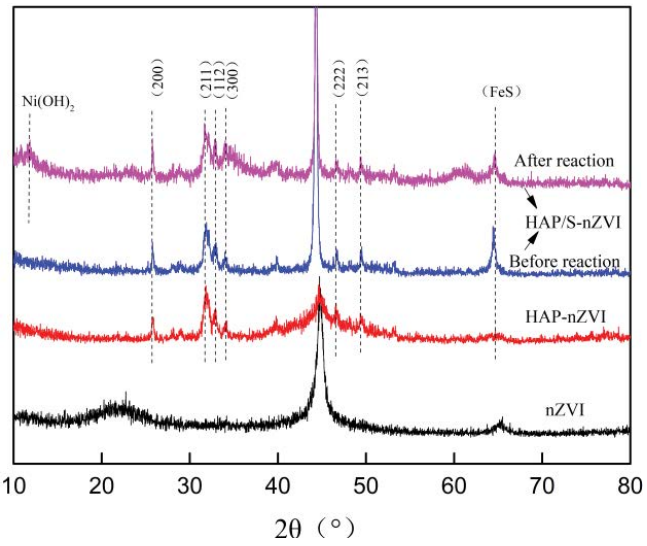

Fig. 7. XRD patterns of nZVI, HAP/nZVI and HAP/S-nZVI.

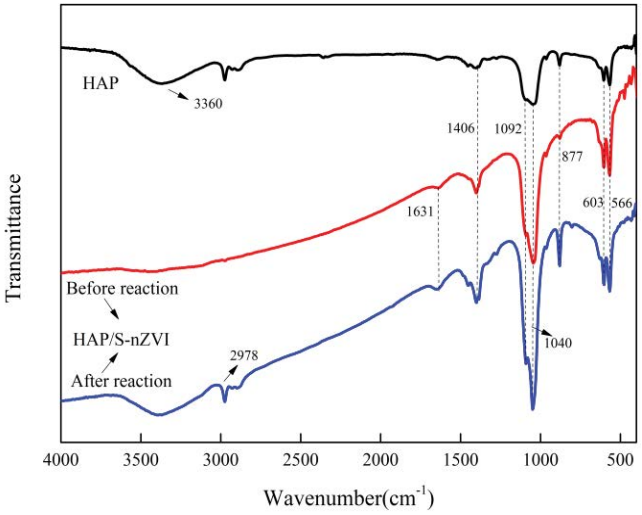

Fig. 8. FTIR spectra of HAP, and HAP/S-nZVI composite (before and after reaction).

indicated the presence of Fe^0, and corresponded to the two indexed (110) and (200) planes of Fe [20,36]. Peaks at 2θ of 44.69°, 65.11° and 84.47° were assigned to be the result of oxidation during synthesis. For HAP/nZVI and HAP/S-nZVI before the reaction, the typical peak at 2θ = 65.5° was assigned to FeS, implying that FeS was synthesized in the process of sulfide modification [20,28,45]. Combined with TEM image and EDX spectrum, the existence of surface FeS of zero-valent nanoparticles is proved. For HAP/S-nZVI after the reaction, a new peak detected at 2 h = 10°–15° was assigned to $Ni(OH)_2$, suggesting that part of Ni(II) is adsorbed in the form of precipitation [7]. In addition, in the XRD pattern of HAP/nZVI and HAP/S-nZVI, The characteristic peaks at 26°, 32°, 33°, 34°, 46.7° and 49° corresponded to the (002), (211), (112), (300), (222) and (213) lattice planes of HAP [43].

The FTIR data of various materials are shown in Fig. 8. For HAP, these peaks can be regarded as representative peaks, including 566, 603, 877, 1,040 and 1,092 cm^{-1} [42]. The peaks at 2,978 and 1,406 cm^{-1} are considered as stretching vibration peak of $–CH_2–$. The broadband at 3,360 cm^{-1} in the samples were related to –OH vibration. Bending vibration of bound water on materials surface is specified at 1,631 cm^{-1}. In addition, the –OH peak of the composites was almost disappeared before the reaction, the probable reason is that HAP was coated by nanometer zero-valent iron modified by sulfur during the preparation process, After the reaction, the –OH peak appears at 3,360 cm^{-1}, which also indicates that the surface coated S-nZVI is involved in the reaction, and there may be $Ni(OH)_2$ precipitation on the surface.

3.9. Proposed reaction mechanism

XPS analysis was performed to further clarify the surface information about the elemental valence states of HAP/S-nZVI. The XPS spectra illustrated that Fe, C, O and S were the primary elements in all samples, and the photoelectron lines at binding energies of ~720 eV, ~288 eV, ~534 eV and ~166 eV were related to Fe 2p, C 1s, O 1s and S 2p, correspondingly. After Ni(II) capture, the new peak at 855eV was attributed to Ni 2p, suggesting Ni was immobilized to the surface of the material (Fig. 9a). The detailed XPS of Fe 2p before and after the reaction is shown in Fig. 9c and d. The Fe 2p XPS survey spectrum showed peaks at 712 and 724 eV that were assigned Fe $2p_{3/2}$ and Fe $2p_{1/2}$ of Fe(III)-O, respectively [27]. The Fe 2p peak at 710 eV corresponded to Fe $2p_{3/2}$ for Fe(II)-O, and the peak at 711 eV was attributed to Fe $2p_{3/2}$ from Fe(II)-S. There is no Fe^0 peak at 706 eV before and after the reaction, which indicates that the surface of nZVI is shielded by a thin layer of iron oxide or iron sulfide [7,46]. The peak of FeS/Fe(II) before the reaction was significantly higher than that after the reaction, indicating that FeS was involved in the reaction. Fig. 9e and f are the XPS spectra of S 2p before and after the reaction. The XPS spectrum of S 2p (Fig. 9c) had two broad peaks around 168.9 and 162.1 eV for HAP/S-nZVI before reaction, which were the characteristic peaks of SO_4^{2-} and S^{2-}, respectively. For the HAP/S-nZVI after reaction, the characteristic peak corresponding to S^0 (164.3 eV) was observed, that means S^{2-} is oxidized to S^0, the oxidation could be caused by Fe^{3+} and dissolved oxygen in the solution [Eqs. (21) and (22)] [19,47]. As shown in Fig. 9b, the peak value of Ni 2p at 847 eV corresponds to Ni $2p_{3/2}$ of NiS, while the peak value of 855.4 eV corresponds to Ni(II)-OH, in addition, it corresponds to Ni(II)-O at 862 eV. and the peak at 877 eV is attributed to Ni $2p_{1/2}$. In addition, two intense peaks for Ni $2p_{1/2}$ were observed at 880 and 873 eV, respectively, with the peak spacing is 7.0 eV, indicating the Ni(II) structure is bonded to HAP/S-nZVI, which were in accordance with those reported for Ni(II) in literature [48]. From the changes in peak intensity before and after the Fe 2p and S 2p reactions, combined with Figs. 9b and 3, it is proved that FeS participates in the elimination of Ni(II), Removal of highly toxic Ni(II) by methods of co-precipitation and reaction, the other part is reduced by Fe^0 to the less toxic Ni^0. However, there is no Ni^0 after the reaction, which may be caused by S^0 reaction [Eq. (23)] [49].

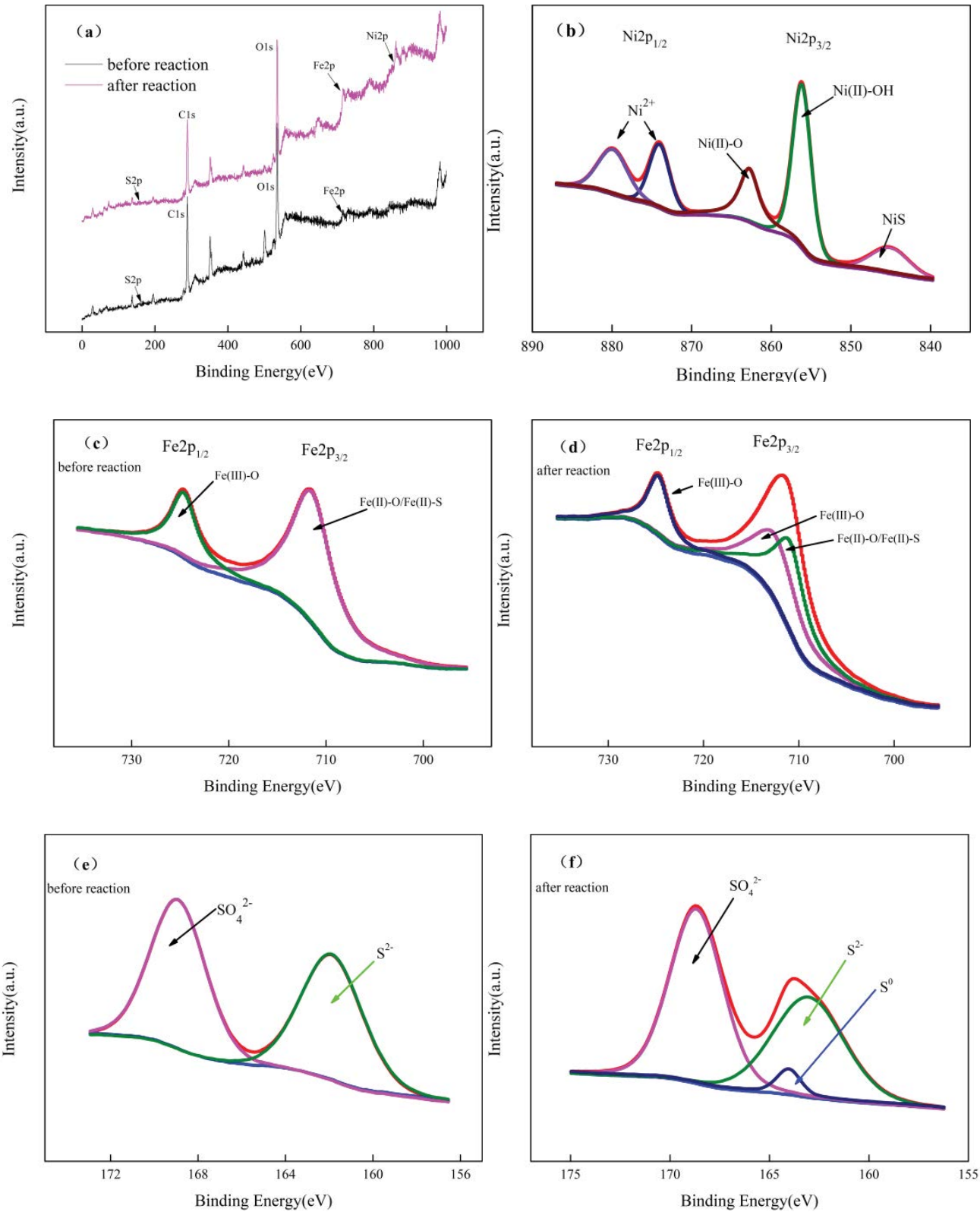

Fig. 9. (a) XPS spectrum, (b) Ni 2p (after reaction), (c) Fe 2p (before reaction), (d) Fe 2p (after reaction), (e) S 2p (before reaction) and (f) S 2p (after reaction).

$$S^{2-} + 1/2O_2 + H^+ \rightarrow S^0 + OH^- \quad (21)$$

$$S^{2-} + 2Fe^{3+} \rightarrow S^0 + 2Fe^{2+} \quad (22)$$

$$S^0 + Ni^0 \rightarrow NiS \quad (23)$$

XPS analysis indicated that Ni(II) had a valence state change and successfully fixed on HAP/S-nZVI. Other studies have shown that FeS has a low zero charge point pH (pH_{PZC}) (2.9) and is more likely to adsorb cations through electrostatic gravity than Fe^0 (7.5), which can promote cation adsorption through electrostatic attraction [36,49]. Thus, the FeS_x layer could facilitate the transfer of electrons from Fe^0 to the chemisorbed Ni(II).

Because the solubility product constant of NiS (K_{sp} = 1.07 × 10^{-21}) is lower than that of FeS (K_{sp} = 1.59 × 10^{-19}), Substitution reaction and surface complexation are the main removal methods [Eqs. (28) and (29)] and Eq. (32) [47,50]. The presence of SO_4^{2-} before and after the reaction (Fig. 9e and f), part of which may be the adsorption of SO_4^{2-} by oxides on the surface of S-nZVI. NiS has low stability, making S^{2-} easier to be oxidized to SO_4^{2-}. The following type: [Eqs. (24) and (25)] and Eq. (10) [47].

$$S^0 + 4H_2O + 6Fe^{3+} \rightarrow SO_4^{2-} + 6Fe^{2+} + 8H^+ \quad (24)$$

$$S^{2-} + 4H_2O + 8Fe^{3+} \rightarrow SO_4^{2-} + 8Fe^{2+} + 8H^+ \quad (25)$$

According to the above solid phase and solution analysis, the possible reaction mechanism for the removal of Ni(II) by HAP/S-nZVI was proposed (Fig. 10), including electrostatic adsorption, reduction and surface complexation [50].

On the basis of the results analyzed above, Ni(II) could be fixed on HAP/S-nZVI through the following reactions:

- Reaction with nZVI
  Surface complexation:

$$Fe^0 + Ni^{2+} \rightarrow Fe^{2+} + Ni^0 \quad (26)$$

$$\equiv Fe^+ + H_2O \rightarrow \equiv FeOH + H^+ \quad (27)$$

$$\equiv Fe0^- + Ni^{2+} \rightarrow FeONi^+ \quad (28)$$

$$\equiv FeOH + Ni^{2+} + H_2O \rightarrow \equiv FeONiOH + 2H^+ \quad (29)$$

- Reaction with FeS
  Chemical precipitation:

$$FeS + H^+ \rightarrow Fe^{2+} + HS^- \quad (30)$$

$$Ni^{2+} + HS^- \rightarrow NiS(s) + H^+ \quad (31)$$

$$FeS(s) + Ni^{2+} \rightarrow NiS(s) + Fe^{2+} \quad (32)$$

Surface complexation:

$$\equiv FeS(s) + Ni^{2+} \rightarrow \equiv FeS - Ni^{2+} \quad (33)$$

4. Conclusions

In this study, HAP/S-nZVI was successfully prepared through a one-step method and used to remove Ni(II) from aqueous solution. The results showed that sulfide modification and dispersion by HAP can effectively enhanced nZVI reactivity and presented synergistic effect towards removal Ni(II). The excellent behaviors of short equilibrium time (15 min for equilibrium), high removal efficiency

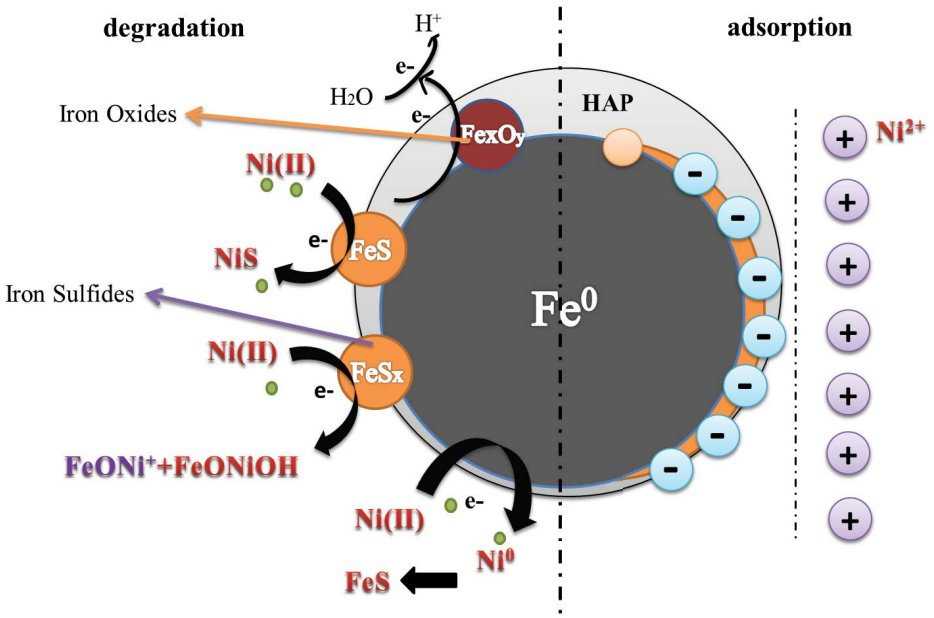

Fig. 10. Proposed degradation pathways for Ni(II) degradation.

(98.25%, HAP/S-nZVI (1:0.5) after 15 min) and high adsorption capacity (302.27 mg g^{-1} at pH = 7 and 298 K) revealed the outstanding performances of HAP/S-nZVI in Ni(II) removal. The stability experiments and dynamic system investigations further illustrated its potential ability for real applications. Characterization results revealed that the Ni(II) was immobilized through surface complexation, electrostatic attraction and reduction of zero-valent iron, as evidenced by change in valence state. The Ni(II) immobilization on HAP/S-nZVI was an endothermic process, and it was well described by pseudo-second-order kinetic model and Freundlich isotherm model. Moreover, the possible elimination mechanism confirmed adsorption and reduction were both involved in the removal process. This paper emphasized that the sulfur-modified nanometer zero-valent iron supported by hydroxyapatite is a promising adsorption material for the remediation of heavy metals.

Acknowledgements

This work was supported by the National Natural Science Foundation of China (NSFC) (51763015, 51663014), the Program for Hongliu First-class Discipline Construction in Lanzhou University of Technology.

References

[1] L.T.M. Thy, N.H. Kiem, T.H. Tu, L.M. Phu, D.T.Y. Oanh, H.M. Nam, M.T. Phong, N.H. Hieu, Fabrication of manganese ferrite/graphene oxide nanocomposites for removal of nickel ions, methylene blue from water, Chem. Phys., 533 (2020) 110700, doi: 10.1016/j.chemphys.2020.110700.

[2] Z.F. Li, H.P. Dong, Y.L. Zhang, J.F. Li, Y.M. Li, Enhanced removal of Ni(II) by nanoscale zero valent iron supported on Na-saturated bentonite, J. Colloid Interface Sci., 497 (2017) 43–49.

[3] K.S. Yoon, D.-W. Cho, A. Bhatnagar, H. Song, Adsorption of As(V) and Ni(II) by Fe-Biochar composite fabricated by co-pyrolysis of orange peel and red mud, Environ. Res., 188 (2020) 109809, doi: 10.1016/j.envres.2020.109809.

[4] M.B. Porto, L.B. Alvim, A.F. de Almeida Neto, Nickel removal from wastewater by induced co-deposition using tungsten to formation of metallic alloys, J. Cleaner Prod., 142 (2017) 3293–3299.

[5] M.P. Aji, P.A. Wiguna, J. Karunawan, A.L. Wati, Sulhadi, Removal of heavy metal nickel-ions from wastewaters using carbon nanodots from frying oil, Procedia Eng., 170 (2017) 36–40.

[6] J. Liu, A.R. Liu, W.-X. Zhang, The influence of polyelectrolyte modification on nanoscale zero-valent iron (nZVI): aggregation, sedimentation, and reactivity with Ni(II) in water, Chem. Eng. J., 303 (2016) 268–274.

[7] T.-H. Tsai, H.-W. Chou, Y.-F. Wu, Removal of nickel from chemical plating waste solution through precipitation and production of microsized nickel hydroxide particles, Sep. Purif. Technol., 251 (2020) 117315, doi: 10.1016/j.seppur.2020.117315.

[8] F.S. Hoseinian, B. Rezai, E. Kowsari, A. Chinnappan, S. Ramakrishna, Synthesis and characterization of a novel nanocollector for the removal of nickel ions from synthetic wastewater using ion flotation, Sep. Purif. Technol., 240 (2020) 116639, doi: 10.1016/j.seppur.2020.116639.

[9] F.S. Hoseinian, B. Rezai, M. Safari, D. Deglon, E. Kowsari, Effect of hydrodynamic parameters on nickel removal rate from wastewater by ion flotation, J. Environ. Manage., 244 (2019) 408–414.

[10] M. Xu, J.S. Liu, K.Y. Hu, C.Y. Xu, Y.Y. Fang, Nickel(II) removal from water using silica-based hybrid adsorbents: fabrication and adsorption kinetics, Chin. J. Chem. Eng., 24 (2016) 1353–1359.

[11] D. Anitha, A. Ramadevi, R. Seetharaman, Biosorptive removal of Nickel(II) from aqueous solution by Mangosteen shell activated carbon, Mater. Today:. Proc., 45 (2021) 718–722.

[12] B.Y. Qin, H.P. Luo, G.L. Liu, R.D. Zhang, S.S. Chen, Y.P. Hou, Y. Luo, Nickel ion removal from wastewater using the microbial electrolysis cell, Bioresour. Technol., 121 (2012) 458–461.

[13] W.B. Wang, P.P. Zhao, Y.F. Hu, R.X. Zan, Application of weak magnetic field coupling with zero-valent iron for remediation of groundwater and wastewater: a review, J. Cleaner Prod., 262 (2020) 121341, doi: 10.1016/j.jclepro.2020.121341.

[14] S. Vasarevičius, V. Danila, D. Paliulis, Application of stabilized nano zero valent iron particles for immobilization of available Cd^{2+}, Cu^{2+}, Ni^{2+}, and Pb^{2+} ions in soil, Int. J. Environ. Res., 13 (2019) 465–474.

[15] M. Malakootian, M. Daneshkhah, H. Hossaini, Removal of phosphates from aqueous solution by sepiolite-nano zero valent iron composite optimization with response surface methodology, Int. J. Environ. Sci. Technol., 15 (2018) 2129–2140.

[16] W.J. Xu, X.Y. Hu, Y.L. Lou, X.D. Jiang, K.K. Shi, Y.N. Tong, X.H. Xu, C.F. Shen, B.L. Hu, L.P. Lou, Effects of environmental factors on the removal of heavy metals by sulfide-modified nanoscale zerovalent iron, Environ. Res., 187 (2020) 109662, doi: 10.1016/j.envres.2020.109662.

[17] D. Lv, J.S. Zhou, Z. Cao, J. Xu, Y.L. Liu, Y.Z. Li, K.L. Yang, Z. Lou, L.P. Lou, X.H. Xu, Mechanism and influence factors of chromium(VI) removal by sulfide-modified nanoscale zerovalent iron, Chemosphere, 224 (2019) 306–315.

[18] D. Lv, X.X. Zhou, J.S. Zhou, Y.L. Liu, Y.Z. Li, K.L. Yang, Z.M. Lou, S.A. Baig, D.L. Wu, X.H. Xu, Design and characterization of sulfide-modified nanoscale zerovalent iron for cadmium(II) removal from aqueous solutions, Appl. Surf. Sci., 442 (2018) 114–123.

[19] S.S. Liu, H.P. Feng, L. Tang, H.R. Dong, J.J. Wang, J.F. Yu, C.Y. Feng, Y. Liu, T. Luo, T. Ni, Removal of Sb(III) by sulfidated nanoscale zerovalent iron: the mechanism and impact of environmental conditions, Sci. Total Environ., 736 (2020) 139629, doi: 10.1016/j.scitotenv.2020.139629.

[20] J. Duan, H.D. Ji, W. Liu, X. Zhao, B. Han, S.T. Tian, D.Y. Zhao, Enhanced immobilization of U(VI) using a new type of FeS-modified Fe0 core-shell particles, Chem. Eng. J., 359 (2019) 1617–1628.

[21] M.H. Su, D.C.W. Tsang, X.Y. Ren, Q.P. Shi, J.F. Tang, H.G. Zhang, L.J. Kong, L. Hou, G. Song, D.Y. Chen, Removal of U(VI) from nuclear mining effluent by porous hydroxyapatite: evaluation on characteristics, mechanisms and performance, Environ. Pollut., 254 (2019) 112891, doi: 10.1016/j.envpol.2019.07.059.

[22] A.S. Berlyand, A.P. Snyakin, A.A. Prokopov, Adsorption capacity of hydroxyapatite for several amino acids and heavy metal ions, Pharm. Chem. J., 46 (2012) 292–294.

[23] A. Martínez-Olivas, J. Torres-Pérez, P. Balderas-Hernández, S.Y. Reyes-López, Oxytetracycline sorption onto synthetized materials from hydroxyapatite and aluminosilicates, Water Air Soil Pollut., 231 (2020), doi: 10.1007/s11270-020-04638-3.

[24] S. Pai, M. Srinivas Kini, R. Selvaraj, A review on adsorptive removal of dyes from wastewater by hydroxyapatite nanocomposites, Environ. Sci. Pollut. Res., 28 (2019) 11835–11849.

[25] Y.M. Li, Y. Zhang, Y. Zhang, G.X. Wang, S.Y. Li, R.M. Han, W. Wei, Reed biochar supported hydroxyapatite nanocomposite: characterization and reactivity for methylene blue removal from aqueous media, J. Mol. Liq., 263 (2018) 53–63.

[26] A. Phasuk, S. Srisantitham, T. Tuntulani, W. Anutrasakda, Facile synthesis of magnetic hydroxyapatite-supported nickel oxide nanocomposite and its dye adsorption characteristics, Adsorption, 24 (2018) 157–167.

[27] J.K. Du, J.G. Bao, X.Y. Fu, C.H. Lu, S.H. Kim, Mesoporous sulfur-modified iron oxide as an effective Fenton-like catalyst for degradation of bisphenol A, Appl. Catal., B, 184 (2016) 132–141.

[28] M.J. Deng, X.J. Wang, Y. Li, F. Wang, Z.W. Jiang, Y.Y. Liu, Z.L. Gu, S.Q. Xia, J.F. Zhao, Reduction and immobilization of Cr(VI) in aqueous solutions by blast furnace slag supported sulfidized nanoscale zerovalent iron, Sci. Total Environ., 743 (2020) 140722, doi: 10.1016/j.scitotenv.2020.140722.

[29] Y.F. Lam, L.Y. Lee, S.J. Chua, S.S. Lim, S.Y. Gan, Insights into the equilibrium, kinetic and thermodynamics of nickel removal by environmental friendly *Lansium domesticum* peel biosorbent, Ecotoxicol. Environ. Saf., 127 (2016) 61–70.
[30] N. Samadi, R. Ansari, B. Khodavirdilo, Synthesized nano particle derivation of poly (Styrene – co-Maleic Anhydride) and sour cherry rock for removing nickel(II) ion from aqueous solutions, Toxicol. Rep., 6 (2019) 590–597.
[31] S. Agarwal, I. Tyagi, V.K. Gupta, M.H. Dehghani, J. Jaafari, Rapid removal of noxious nickel (II) using novel γ-alumina nanoparticles and multiwalled carbon nanotubes: kinetic and isotherm studies, J. Mol. Liq., 224 (2016) 618–623.
[32] Z.H. Zhang, X.J. Wang, H. Wang, J.F. Zhao, Removal of Pb(II) from aqueous solution using hydroxyapatite/calcium silicate hydrate (HAP/C-S-H) composite adsorbent prepared by a phosphate recovery process, Chem. Eng. J., 344 (2018) 53–61.
[33] Y.J. Cheng, H.R. Dong, Y. Lu, K.J. Hou, Y.Y. Wang, Q. Ning, L. Li, B. Wang, L.H. Zhang, G.M. Zeng, Toxicity of sulfide-modified nanoscale zero-valent iron to *Escherichia coli* in aqueous solutions, Chemosphere, 220 (2019) 523–530.
[34] Y.J. Li, X.G. Zhao, Y. Yan, J.F. Yan, Y.T. Pan, Y.H. Zhang, B. Lai, Enhanced sulfamethoxazole degradation by peroxymonosulfate activation with sulfide-modified microscale zero-valent iron (S-mFe^0): performance, mechanisms, and the role of sulfur species, Chem. Eng. J., 376 (2019) 121302, doi: 10.1016/j.cej.2019.03.178.
[35] B. Wang, H.R. Dong, L. Li, Y.Y. Wang, Q. Ning, L. Tang, G.M. Zeng, Influence of different co-contaminants on trichloroethylene removal by sulfide-modified nanoscale zero-valent iron, Chem. Eng. J., 381 (2020) 122773, doi: 10.1016/j.cej.2019.122773.
[36] J. Gao, L.Z. Yang, Y.Y. Liu, F.L. Shao, Q.H. Liao, J.G. Shang, Scavenging of Cr(VI) from aqueous solutions by sulfide-modified nanoscale zero-valent iron supported by biochar, J. Taiwan Inst. Chem. Eng., 91 (2018) 449–456.
[37] R.B. Fu, Y.P. Yang, Z. Xu, X. Zhang, X.P. Guo, D.S. Bi, The removal of chromium(VI) and lead(II) from groundwater using sepiolite-supported nanoscale zero-valent iron (S-nZVI), Chemosphere, 138 (2015) 726–734.
[38] A.N. Garcia, H.K. Boparai, C.V. de Boer, A.I.A. Chowdhury, C.M.D. Kocur, L.M. Austrins, J. Herrera, D.M. O'Carroll, Fate and transport of sulfidated nano zerovalent iron (S-nZVI): a field study, Water Res., 170 (2020) 115319, doi: 10.1016/j.watres.2019.115319.
[39] H. Xu, W.G. Tian, Y.J. Zhang, J. Tang, Z.T. Zhao, Y. Chen, Reduced graphene oxide/attapulgite-supported nanoscale zero-valent iron removal of Acid Red 18 from aqueous solution, Water Air Soil Pollut., 229 (2018) 1–16, doi: 10.1007/s11270-018-4033-5.
[40] H. Xu, Y.J. Zhang, Y. Chen, W.G. Tian, Z.T. Zhao, J. Tang, Polyaniline/attapulgite-supported nanoscale zero-valent iron for the rival removal of azo dyes in aqueous solution, Adsorpt. Sci. Technol., 37 (2019) 1–19, doi: 10.1177/0263617418822917.
[41] Y. Chen, Z.H. Lin, R.R. Hao, H. Xu, C.Y. Huang, Rapid adsorption and reductive degradation of Naphthol Green B from aqueous solution by Polypyrrole/Attapulgite composites supported nanoscale zero-valent iron, J. Hazard. Mater., 371 (2019) 8–17.
[42] Y. Liu, Is the free energy change of adsorption correctly calculated?, J. Chem. Eng. Data, 54 (2009) 1981–1985.
[43] Y.M. Li, S.Y. Wang, Y. Zhang, R.M. Han, W. Wei, Enhanced tetracycline adsorption onto hydroxyapatite by Fe(III) incorporation, J. Mol. Liq., 247 (2017) 171–181.
[44] H.L. Fan, H.Y. Ren, X.Z. Ma, S.F. Zhou, J. Huang, W.Z. Jiao, G.S. Qi, Y.Z. Liu, High-gravity continuous preparation of chitosan-stabilized nanoscale zero-valent iron towards Cr(VI) removal, Chem. Eng. J., 390 (2020) 124639, doi: 10.1016/j.cej.2020.124639.
[45] Q. Bin, B. Lin, K. Zhu, Y.Q. Shen, Y.Y. Man, B.Y. Wang, C.F. Lai, W.J. Chen, Superior trichloroethylene removal from water by sulfide-modified nanoscale zero-valent iron/graphene aerogel composite, J. Environ. Sci., 88 (2020) 90–102.
[46] Y.-h. Zhang, F.-q. Liu, C.-q. Zhu, X.-p. Zhang, M.-m. Wei, F.-h. Wang, C. Ling, A.-m. Li, Multifold enhanced synergistic removal of nickel and phosphate by a (N,Fe)-dual-functional bio-sorbent: mechanism and application, J. Hazard. Mater., 329 (2017) 290–298.
[47] L. Liang, X.Q. Li, Y.Q. Guo, Z. Lin, X.T. Su, B. Liu, The removal of heavy metal cations by sulfidated nanoscale zero-valent iron (S-nZVI): the reaction mechanisms and the role of sulfur, J. Hazard. Mater., 404 (2021) 124057, doi: 10.1016/j.jhazmat.2020.124057.
[48] O.A. Oyewo, B. Mutesse, T.Y. Leswifi, M.S. Onyango, Highly efficient removal of nickel and cadmium from water using sawdust-derived cellulose nanocrystals, J. Environ. Chem. Eng., 7 (2019) 103251, doi: 10.1016/j.jece.2019.103251.
[49] A.M. Widler, T.M. Seward, The adsorption of gold(I) hydrosulphide complexes by iron sulphide surfaces, Geochim. Cosmochim. Acta, 66 (2002) 383–402.
[50] X.L. Zhao, Y. Wang, H.Y. Wu, L.C. Fang, J.J. Liang, Q.H. Fan, P. Li, Insights into the effect of humic acid on Ni(II) sorption mechanism on illite: batch, XPS and EXAFS investigations, J. Mol. Liq., 248 (2017) 1030–1038.

Supplementary information

S1. Tafel curve test method

The electrochemical properties of S-nZVI and nZVI were measured by Tafel curves at an electrochemical workstation (CHI660D). A three-electrode battery system (working electrode, calomel electrode and platinum electrode) was used to detect NaCl solution with a concentration of 3.5%. Immediately measure the Tafel curve. The corrosion current was obtained by fitting the curve. To observe the electrochemical properties of the material.

Table S1
Instantaneous rates of different adsorbents

c_0 (mg L^{-1})	Time (min)	HAP (mg g^{-1} min^{-1})	nZVI (mg g^{-1} min^{-1})	HAP/nZVI (mg g^{-1} min^{-1})	HAP/S-nZVI (S/Fe = 0.1) (mg g^{-1} min^{-1})	HAP/S-nZVI (S/Fe = 0.3) (mg g^{-1} min^{-1})	HAP/S-nZVI (S/Fe = 0.5) (mg g^{-1} min^{-1})
50	1	16.2716	18.1605	21.4012	22.6296	22.4630	22.5802
	3	1.5740	0.8209	1.4136	1.2716	1.1111	1.0679
	5	0.8074	0.4963	0.5741	0.3494	0.6642	0.5185
	10	0.0333	0.1988	0.1852	0.0284	0.0210	0.0914
	20	0.1086	0.0963	0.0283	0.0099	0.0148	0.0049
	30	0.063	0.0432	0.0045	0.0037	0.0037	0.0008
	45	0.0428	0.0090	0.0008	0.0008	0.0008	0.0006
	60	0.0313	0.0033	0	0.0006	0.0016	0.0003

Table S2
Comparison of different materials on removal of Ni(II)

Adsorbents	Ni(II) initial concentration (mg L^{-1})	Temperature (°C)	Time (min)	Dosage of adsorbent (g L^{-1})	pH	Removal rate (%)	reference
HAP/S-nZVI	50	25	10	0.1	3–9	98.25	This work
nZVI/Na-bent	200	25	60	0.78	8	98.50	[2]
Anionic polyacrylamide (APAM)-nZVI	100	25	15	0.05	6.4	80	[6]
Carboxymethylcellulose sodium (CMC)-nZVI			30	1 g		>95	
Lansium domesticum peel biosorbent	40	30	20	6 g	6	96	[29]
Poly(styrene-co-maleic anhydride) modified MelamineOxalic acid	50	25	90	1.5	6	>99	[30]
Multiwalled carbon nanotubes	75	25	30	0.3	10	88	[31]
Amino functionalized graphene oxide	10	–	10	0.1	9	≈100	[8]

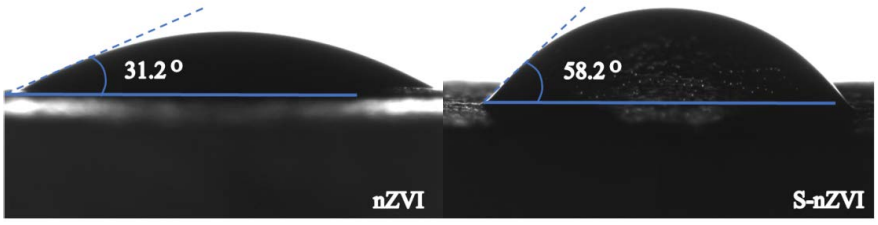

Fig. S1. The contact angle between nZVI and S-nZVI.

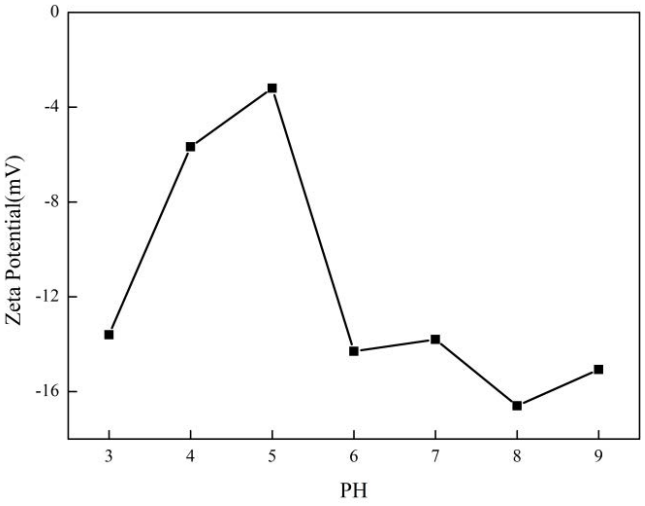

Fig. S2. Zeta (ζ) potential of the HAP/S-nZVI.

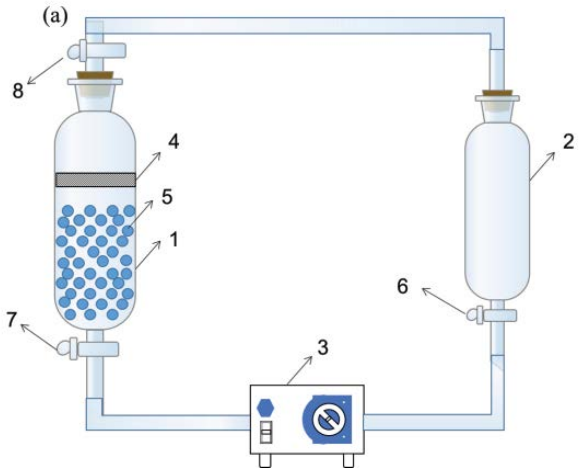

Fig. S3. Diagram of dynamic adsorption unit (1, 2-glass tube; 3-peristaltic pump; 4-perforated baffle; 5-glass bead; 6, 7, 8-piston) (basic conditions: T = 298 K, initial pH = 7.0, 500 mL of 50 mg L^{-1} Ni(II) solution , 1 g L^{-1} HAP/S-nZVI, 0.5 S/Fe molar ratio, flow range: 0.007–380 mL min^{-1}).

The specific dynamic adsorption test is shown in the Fig. S2. Put the Ni solution in a beaker. Peristatic pump provides power for the solution to pass through the hose through the buffer effect of glass beads, adsorbent for the adsorption experiment (the adsorbent is wrapped by cotton flowers). Observe the influence of speed by controlling the speed of peristaltic pump.

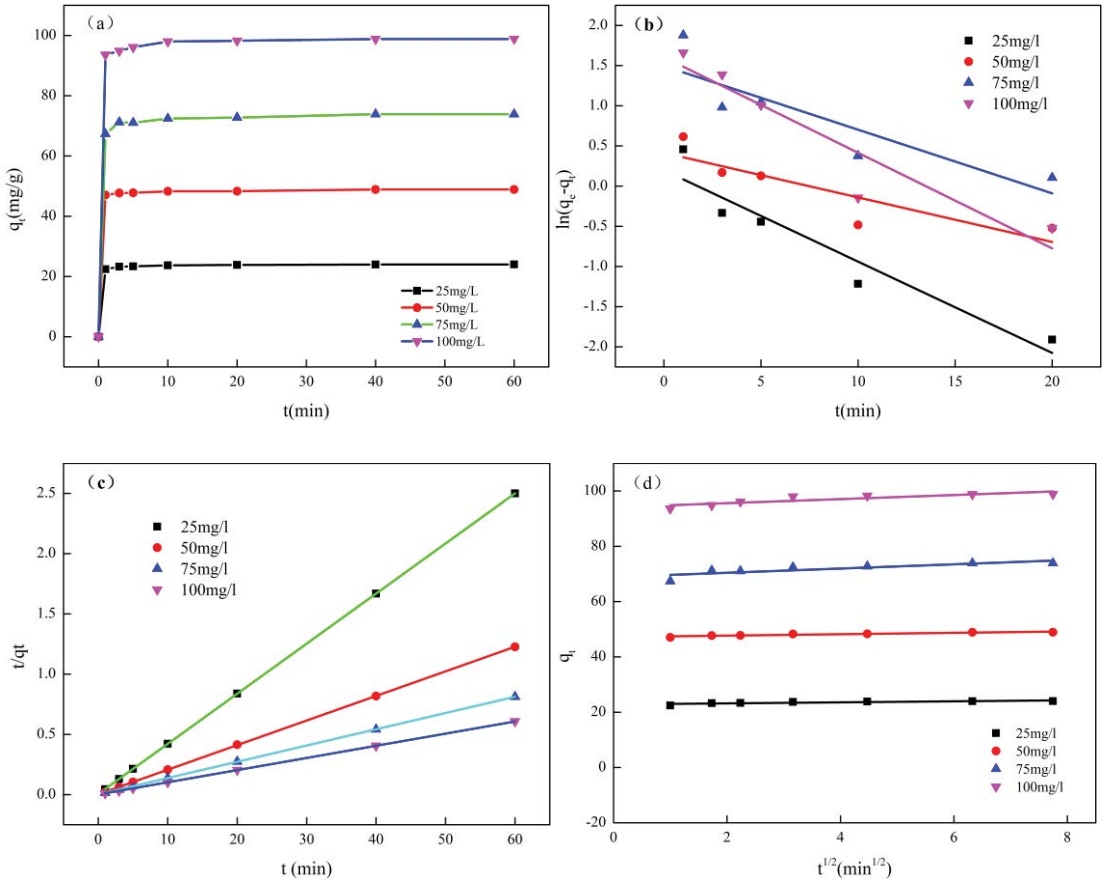

Fig. S4. (a) Adsorption kinetic curve, (b) pseudo-first-order kinetic model, (c) pseudo-second-order kinetic model, and (d) intraparticle diffusion model.

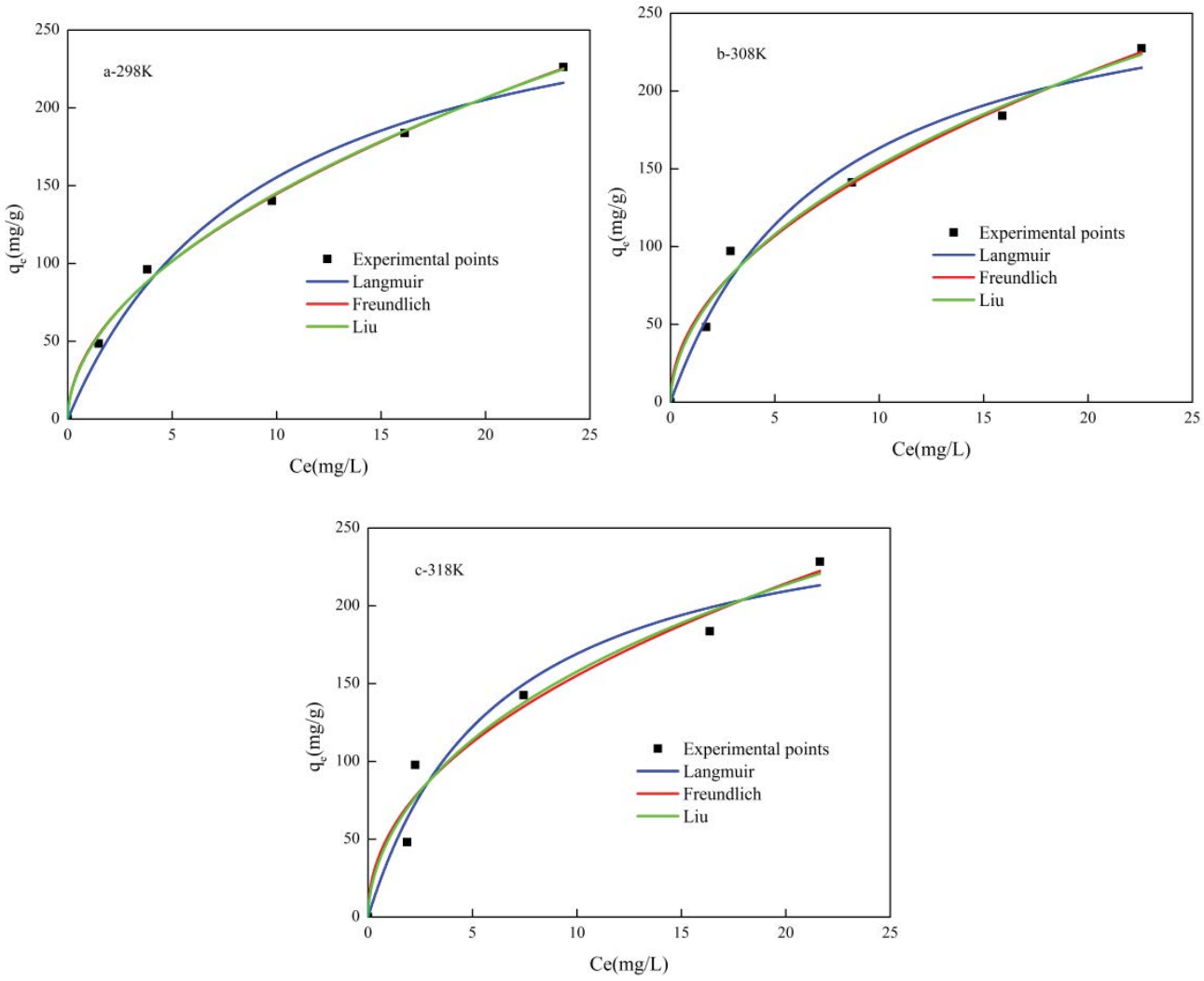

Fig. S5. Equilibrium adsorption isotherms at different temperatures: (a) 298, (b) 308 and (c) 318 K.